

Unclassified


1

2

SECURITY CLASSIFICATION OF THIS PAGE

REPORT DOCUMENTATION PAGE

Form Approved
OMB No. 0704-0188

1a. REPORT SECURITY CLASSIFICATION Unclassified		1b. RESTRICTIVE MARKINGS													
2a. SECURITY CLASSIFICATION AUTHORITY AD-A251 023 		3. DISTRIBUTION / AVAILABILITY OF REPORT Unlimited													
4		5. MONITORING ORGANIZATION REPORT NUMBER(S) AFOSR-89-0340 2 0278													
6a. NAME OF PERFORMING ORGANIZATION Electronics Research Lab	6b. OFFICE SYMBOL (if applicable)	7a. NAME OF MONITORING ORGANIZATION Air Force Office of Scientific Research													
6c. ADDRESS (City, State, and ZIP Code) University of California Berkeley, CA 94720		7b. ADDRESS (City, State, and ZIP Code) Bldg. 410 Bolling Air Force Base, DC 20332-6448													
8a. NAME OF FUNDING / SPONSORING ORGANIZATION AFOSR	8b. OFFICE SYMBOL (if applicable) NE	9. PROCUREMENT INSTRUMENT IDENTIFICATION NUMBER AFOSR-89-0340													
8c. ADDRESS (City, State, and ZIP Code) Bldg. 410 Bolling Air Force Base, DC 20332-6448		10. SOURCE OF FUNDING NUMBERS <table border="1"><tr><td>PROGRAM ELEMENT NO. 61102F</td><td>PROJECT NO. 2301</td><td>TASK NO. AS</td><td>WORK UNIT ACCESSION NO.</td></tr></table>		PROGRAM ELEMENT NO. 61102F	PROJECT NO. 2301	TASK NO. AS	WORK UNIT ACCESSION NO.								
PROGRAM ELEMENT NO. 61102F	PROJECT NO. 2301	TASK NO. AS	WORK UNIT ACCESSION NO.												
11. TITLE (Include Security Classification) Nonlinear Photonics--Limits and Possibilities															
12. PERSONAL AUTHOR(S) T. Kenneth Gustafson															
13a. TYPE OF REPORT Final Report	13b. TIME COVERED FROM 4/1/89 TO 9/30/91	14. DATE OF REPORT (Year, Month, Day) 3/17/91	15. PAGE COUNT 36												
16. SUPPLEMENTARY NOTATION															
17. COSATI CODES <table border="1"><tr><th>FIELD</th><th>GROUP</th><th>SUB-GROUP</th></tr><tr><td> </td><td> </td><td> </td></tr><tr><td> </td><td> </td><td> </td></tr><tr><td> </td><td> </td><td> </td></tr></table>		FIELD	GROUP	SUB-GROUP										18. SUBJECT TERMS (Continue on reverse if necessary and identify by block number)	
FIELD	GROUP	SUB-GROUP													
19. ABSTRACT (Continue on reverse if necessary and identify by block number) Evolving developments in fundamental concepts, materials, and fabrication are making possible new developments and discoveries over a broad spectrum of the nonlinear photonic microstructure field. This includes phenomena associated with sub-micron structures to increase both electronic and photonic confinement, distributed nonlinear photonic interactions in traps and other microstructures, and nonlinear photonic interactions in which the fully quantized nature of the radiation field is important.															
20. DISTRIBUTION / AVAILABILITY OF ABSTRACT <input checked="" type="checkbox"/> UNCLASSIFIED/UNLIMITED <input type="checkbox"/> SAME AS RPT. <input type="checkbox"/> DTIC USERS		21. ABSTRACT SECURITY CLASSIFICATION Unclassified													
22a. NAME OF RESPONSIBLE INDIVIDUAL <i>John S. ...</i>		22b. TELEPHONE (Include Area Code) 22c. OFFICE SYMBOL 202-767-4906 NE													

DTIC
ELECTE
MAY 26 1992
S A DThis document has been approved
for public release and sale; its
distribution is unlimited.

NONLINEAR PHOTONICS—LIMITS AND POSSIBILITIES

FINAL REPORT

Grant No. AFOSR-89-0340

April 1, 1989 to September 30, 1991

T. Kenneth Gustafson
Principal Investigator

Accession For	
NTIS CRA&I	<input checked="checked" type="checkbox"/>
DTIC TAB	<input type="checkbox"/>
Unannounced	<input type="checkbox"/>
Justification	
By	
Distribution /	
Availability	
Dist	Availability / Special
A-1	



92-13056



Department of Electrical Engineering and Computer Sciences
and the Electronics Research Laboratory
University of California, Berkeley, CA 94720

92 5 15 0267

NONLINEAR PHOTONICS-LIMITS AND POSSIBILITIES

T. Kenneth Gustafson

Grant No. AFOSR-89-0340

FINAL REPORT

April 1, 1989 to September 30, 1991

Abstract

Evolving developments in fundamental concepts, materials, and fabrication are making possible new developments and discoveries over a broad spectrum of the nonlinear photonic microstructure field. This includes phenomena associated with sub-micron structures to increase both electronic and photonic confinement, distributed nonlinear photonic interactions in traps and other microstructures, and nonlinear photonic interactions in which the fully quantized nature of the radiation field is important.

In the present report we discuss some of the accomplishments which have occurred as a result of funding by the AFOSR through grant number AFOSR-89-0340. These include tunable Bragg mirrors for microcavities, Aharonov-Bohm photon detectors, four-wave mixing in photorefractive materials, and wide band-gap materials for nonlinear optical interactions at short wavelengths. We also include numerical approaches using the beam propagation method to calculate energy levels in quantum structures and to track from a fundamental point of view the transport of electrons in photonic microstructures. Finally we allude to the role of x-ray optics and collaboration with the x-ray optics center directed by David Attwood.

NONLINEAR PHOTONICS-LIMITS AND POSSIBILITIES

T. Kenneth Gustafson

Grant No. AFOSR-89-0340

FINAL REPORT

April 1, 1989 to September 30, 1991

Introduction

The area of photonic microstructures has been productive both in terms of new phenomena and in terms of new devices. In our own research we have concentrated on several aspects related to both and these are reflected in the results which we discuss in the present report.

Students Supported

- Inho Kim – numerical computation of levels in quantum wells including exciton interactions, computation of second harmonic generation in GaN.
- Khan Nyguyen – photorefractive mixing applied to heterodyne detection, x-ray lithography using a Cassegranian geometry.
- Julie Kenrow – optical spectroscopy of multilayer x-ray mirrors, numerical calculations of coherent electron structures including phonon interactions. Now – a recipient of a Hughes Fellowship award.
- Eddie Yin – Photorefractive mixing at high speed in structured semiconductor photorefractive materials, also has worked on superconducting thin films with support of L.B.L.

Others with independent support who have collaborated

- Olga Blum (Newport Fellow , Tunable Bragg mirror structures, BRAQWET Modulators, Strong Field NLO, in the final year had NSF R. A. support)
- Dave Attwood (X-ray Optics Center LBL [x-ray optics, nanostructures])
- Mike Ruben (Materials Sciences LBL [GaN for harmonic generation])
- R. Neurgaonkar (Rockwell International Sciences Center supplied [SBN])
- Jeniffer Ross (Rockwell Fellow, GaN and II-VI Compounds)
- P. L. Kelley (Lincoln Laboratory,MIT – significant collaboration in applications of renormalization ideas to nonlinear optics)
- Alex Spiridon (Stanford Research Institute- on the development of signal processing ideas related to photorefractive crystals [This is an ongoing effort])
- Jane Zucker (AT&T Bell Laboratories- Holmdel – Has interacted by supervising and directing the modulator and Bragg mirror efforts of Olga Blum)

Overview of Motivation

With the support of the AFOSR we have concentrated on the limits and possibilities associated with photonic microstructures. We have had several reasons for wishing to pursue this area.

- First, the potential in terms of fundamental discovery and the potential for future applications. New electronic and photonic phenomena are being discovered as the scale of photonic devices and structures is reduced.
- Second, historically this is an area in which Berkeley has contributed significantly and has been active. This has been partially because of the interests of the faculty who are there and partially because of the excellent processing capabilities which have existed down to the micron range.
- Third, the outstanding graduate students who are attracted to Berkeley and have interests in this area.

Particular Motivation

There are numerous rather obvious pragmatic reasons for pursuing this particular area.

- As size is reduced the density of devices and their speed are both increased.
- As the size is reduced and the number of electrons participating is also reduced, power requirements and immunity of individual devices to radiation is increased.
- As the number of possible modes for electrons and photons is reduced, there are questions with respect to the coherence of spontaneous processes, and the relationship between stimulated and spontaneous processes. Said otherwise, there are fundamental questions with regard to coherence, particularly with respect to the spontaneous interaction processes.
- The reduction in the scale of devices and the development of basic scientific instrumentation associated with this is an investment in future industrial development, not only in the photonics area but also in the electronics and materials areas.

Finally, from our point of view;

- A truly integrated optical circuit would consist of sub-micron sub-systems separated by less than a wavelength and interconnected optically.

Long Term View

As photonics and electronics develop into the next century, it is becoming more evident that the two fields can be expected to merge. Research in this basic area is an investment which will pay dividends in the decades to come. The DOD has contributed significantly to this evolution by taking a leadership role in directing the research investment, by funding key areas which are impediments to research evolution, and by helping in the training of graduate students in such key areas.

Our Particular Efforts

Our particular results which have been achieved with support of the AFOSR has concentrated on microstructuring, with the long term goal of photonic microstructures in mind. We have carried forward with the plans laid out in the proposal and have numerous students working in diverse areas. The basic areas which have been concentrated upon are shown in Fig.(1). The primary topics have been

- Low photon electron number structures

This has been an effort which Ms. Blum has taken the lead on. She has established an excellent working relationship with Ms. Jane Zucker of AT&T Bell Labs. The primary goal which Ms. Blum has had is to investigate tunable Bragg mirrors for microcavities.

A second aspect of this which has emerged is the use of the "Time Dependent" Aharonov-Bohm Effect for photon detection and in particular quantum non-demolition photon detection. Eddie Yin and Byoungcho Lee have been involved in this effort.

- Diagrams and Linewidth

We have continued to be active in the area of renormalization applied to nonlinear optical calculations. Jointly with P.L. Kelley of Lincoln Laboratory we have coined the term radiative renormalization to such calculations and have recently obtained results to be reported at the Vienna conference (IQEC). The lead student on this activity has been Olga Blum.

- Photorefractive Studies

In the initial proposal we established fundamental studies, diagrams, and materials

as the primary emphasis upon which we would place this effort. The reason that we believed that it should be included is that the role of traps as distributed microstructure interaction sites fits within the preview of photonic microstructures—particularly with some of the more recent work which we are concentrating upon. The lead person in this was initially Khanh Nguyen, and it is now Eddie Yin. We have established a significant interaction with SRI in this effort more recently, particularly with respect to picosecond probing of photorefractive refractive index changes. Khanh has moved into the area of X-ray Optics and is interacting with Dave Attwood and the X-ray optics center as well as with us.

- X-Ray Optical Studies

In the fabrication area we have a long term goal of being able to obtain sub-micron optical devices and systems. Two key ingredients to this are to be able to write patterns and to be able to perform lithography on as small a scale as possible. It has been clear that in the long term x-ray lithography will be an important tool. While optical lithography can be improved somewhat by using phase contrast and other techniques to fabricate sub wave-length optical devices with optical lithography, in the long term shorter wavelengths will be essential.

Dave Attwood and I have been jointly supervising two graduate students in this area—Khanh Nguyen and Max Wei. Both were initially supported with the AFOSR grant but have subsequently been supported with the URI for the x-ray optics center. Their projects are more fully describable as URI projects at this point, however they continue to attend our weekly group meetings and to interact with other students in the group

thereby having considerable influence as to possible future directions, possibilities and goals of their student colleagues.

- Wide Band-gap Materials Studies

With the view of obtaining better materials for short wave-lengths, and to carry out fundamental studies on the harmonic generation of one micron radiation to much shorter wavelengths, we have been studying the growth of epitaxial GaN. This we have been doing jointly with Mike Ruben of the Lawrence Berkeley Laboratory, who has taken the lead in this effort.

We are hoping that we will be able to generate second harmonic radiation using intersub-band transitions in analogy to that which has been accomplished with GaAs at ten microns.

Results and Publications of Results

Main Results

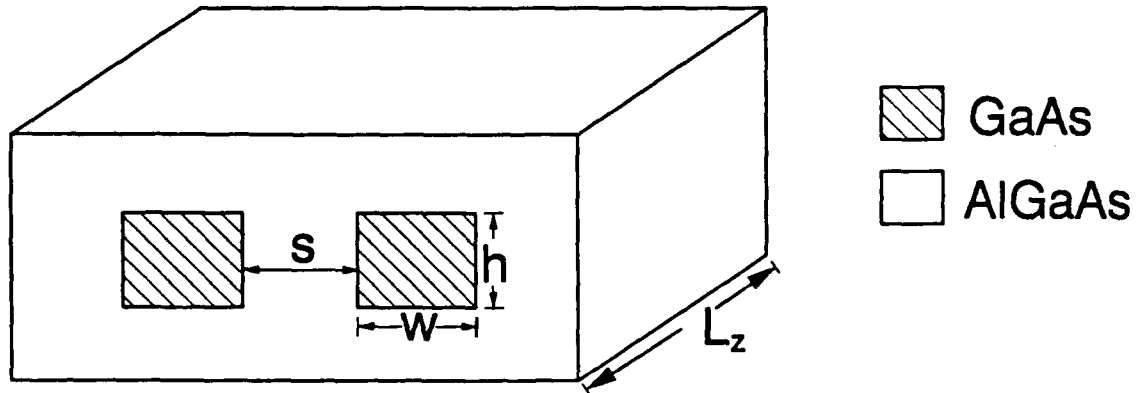
- **Numerical Computation** of Properties of Microstructures Using the Quantum Beam Propagation Method (Inho Kim has completed a Ph.D. thesis based upon this effort (May 1991) High Speed III-V Electro-Optic Modulators and Nonlinear Optical Properties of Quantum Confined Nanostructures)
 - Computation of $\chi^{(2)}$'s for quantum well devices. (Presented at the Hawaii conference on NLO), Figures included.

Publication - (Analysis of Quantum-Confined Structures Using the Beam Propagation Method, *Appl. Phys. Lett.* 53(3),16 July (1990)).

Conclusions

- Presently using the same approach to compute transport properties using the Beam Propagation method. This is recent work on the calculation of electron pulse propagation in wave-guide devices. We are presently in the process of including the electron-phonon scattering mechanisms using the renormalization concepts developed jointly with P. L. Kelley.

ELECTRON QUANTUM WIRE COUPLER



Physical parameters:

$$L_z = 1000 \text{ \AA}$$

$$s = 40 \text{ \AA}$$

$$w = h = 50 \text{ \AA}$$

$$E_{kz} = 0.14 \text{ eV} \quad (v_z = 8 \times 10^5 \text{ m/s})$$

Numerics:

$$N_x = N_y = N_z = 32$$

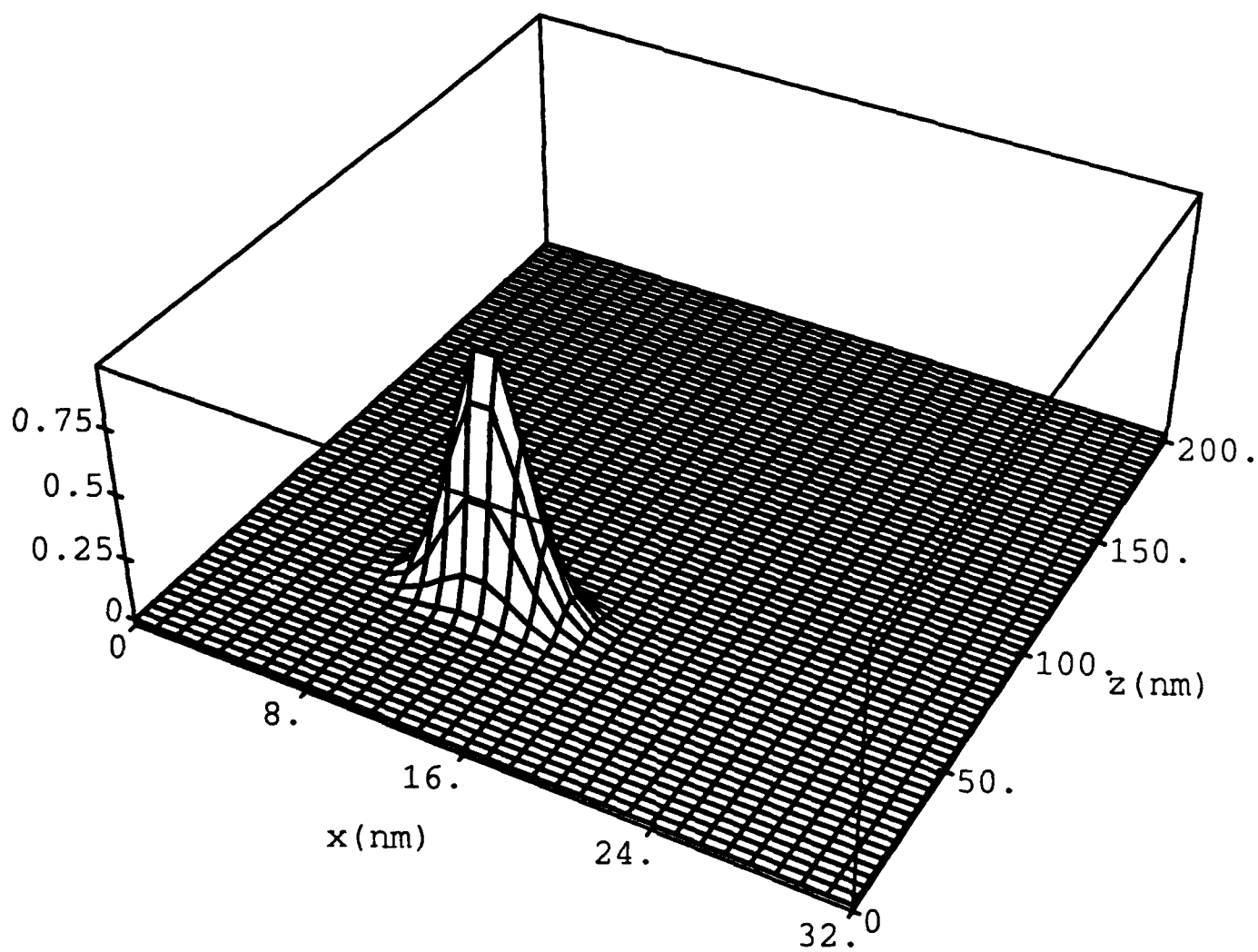
$$N_t = 4000$$

$$\Delta t = 10^{-17} \text{ sec}$$

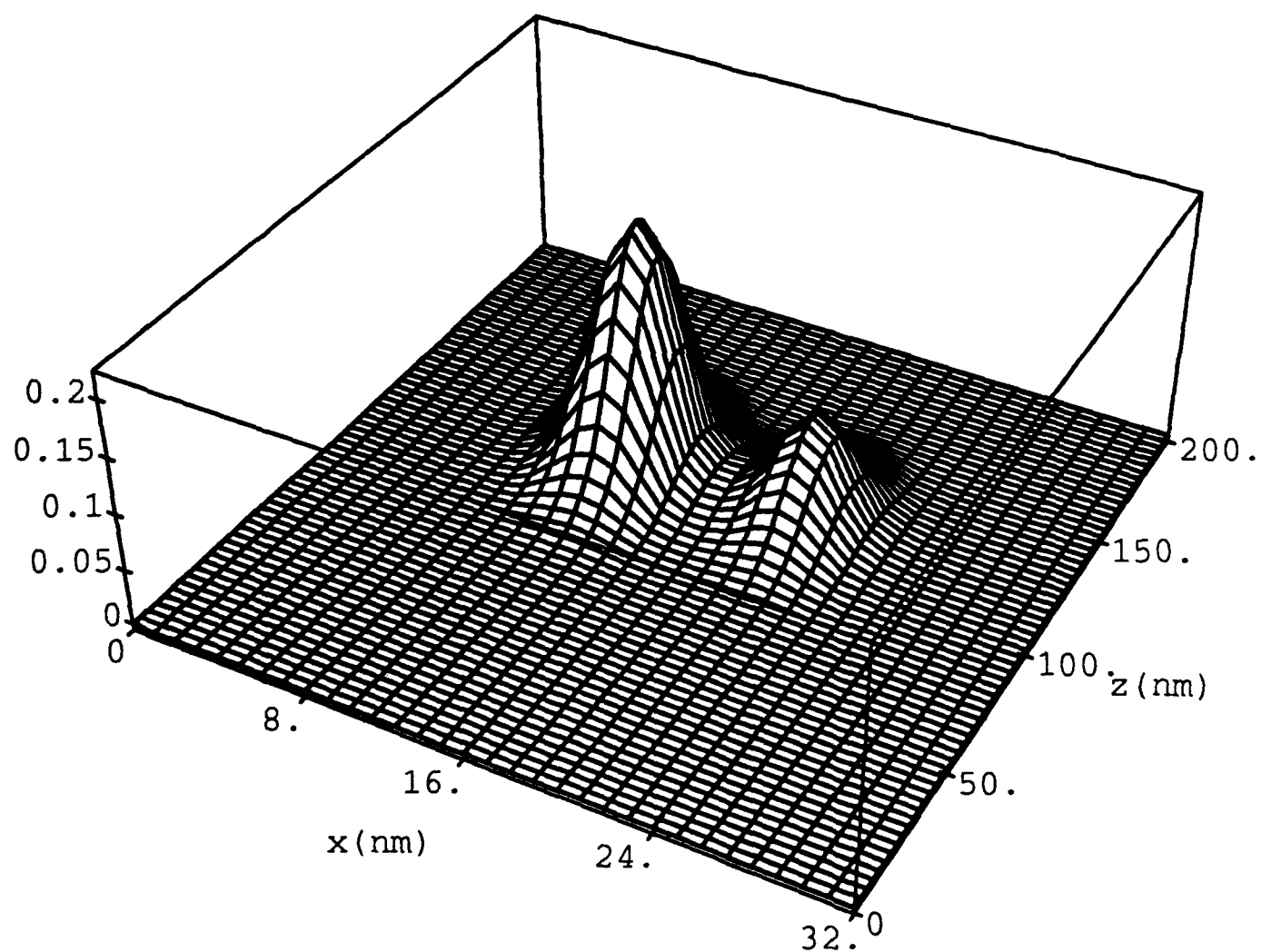
$$\text{Computation time (CPL)} = 22 \text{ hours}$$

(SUN-SPARC 2)

$$|\Psi(x, z)|^2 \text{ at } t = 0$$



$|\Psi(x, z)|^2$ at $t = 40$ fs



Analysis of quantum-confined structures using the beam propagation method

Inho Kim and T. K. Gustafson

Department of Electrical Engineering and Computer Sciences and The Electronics Research Laboratory,
University of California, Berkeley, California 94720

Lars Thylén

Ericsson Telecom AB, S-126 25 Stockholm, Sweden

(Received 5 March 1990; accepted for publication 7 May 1990)

The beam propagation method has been applied to find confined energy eigenvalues and eigenfunctions for a III-V quantum well structure subjected to an external electric field. Quantum-confined Stark shifts for both electrons and holes and excitonic states for single and double quantum wells are calculated. Excellent agreement with analytical results where available is demonstrated. A comparison with experimental data published in the literature is given.

The beam propagation method (BPM) has been applied to numerically solve the scalar wave equation in the paraxial approximation thereby computing modal distributions in optical fibers and various integrated optical devices.^{1,2} Since the relevant differential equations are analogous to Schrödinger type equations, the BPM can be applied directly to solve the time-dependent Schrödinger equation without the paraxial approximation.³ Of particular interest is the Stark effect in quantum-confined nanostructures, such as quantum wells and superlattices, which has thus far been analyzed using the tunneling resonance method, the exact analytical method assuming an infinitely deep well,⁴ and the variational method using the simple solutions for the infinite well case.⁵ A few numerical methods have been reported: the finite element method,⁶ the finite difference method,⁷ and the transfer matrix method.⁸ However, these are time consuming and the spatial dependence of mass due to the heterostructure has either been neglected or taken into account in a tedious way. In this letter it is shown that BPM is convenient for an analysis of the Stark effect of electron and hole states in quantum wells taking mass differences into account. In addition, using the variational method,^{4,9} these results can be used to accurately deduce excitonic effects in quantum well structures.

The basic beam propagation method is well known and described in the literature.¹ Specifically considering a particle in a potential $V(z)$ subjected to an applied electric field E in the z direction, the appropriate time-dependent Schrödinger equation for the envelope wave function in the effective mass approximation is¹⁰

$$i\hbar \frac{\partial}{\partial t} \Psi(z,t) = \left(-\frac{\hbar^2}{2} \frac{\partial}{\partial z} \frac{1}{m^*(z)} \frac{\partial}{\partial z} + V(z) + H'(z) \right) \Psi(z,t), \quad (1)$$

where $H'(z) = -eEz$. It is noted that $(1/m^*)\partial\Psi/\partial z$ is continuous at the interface between two different materials with different masses and hence current conservation is automatically guaranteed. Following the BPM, the wave function $\Psi(z,t + \Delta t)$ is expressed in terms of $\Psi(z,t)$ as

$$\Psi(z,t + \Delta t) = PQP\Psi(z,t) + O((\Delta t)^3), \quad (2)$$

where

$$P = \exp\left(\frac{i}{2} \frac{\Delta t}{\hbar} \frac{\partial}{\partial z} \frac{1}{m^*(z)} \frac{\partial}{\partial z}\right),$$

$$Q = \exp\left(-\frac{i}{\hbar} \int_t^{t+\Delta t} [V(z) + H'(z)] dt\right). \quad (3)$$

In (2), the operator P applied to $\Psi(z,t)$ is equivalent to solving the unperturbed Schrödinger equation over a time interval $\Delta t/2$. This step in the solution can be obtained using a band-limited Fourier series for $\Psi(z,t)$. The P operation then gives

$$P\Psi(z,t) = \frac{1}{N} \sum_{l=-N/2+1}^{N/2} \tilde{\Psi}_l(t) \times \exp\left\{\frac{i}{2} \frac{\Delta t}{\hbar} \left[-\frac{k_z^2}{m^*(z)} + ik_z \left(\frac{\partial}{\partial z} \frac{1}{m^*(z)} \right) \right]\right\} \times \exp\left(i \frac{2\pi lz}{L}\right), \quad (4)$$

where $k_z = 2\pi l/L$, L is the total computational grid size, and $\tilde{\Psi}_l(t)$ is the Fourier component at k_z . This numerical procedure involving P is done efficiently and accurately using the fast Fourier transform (FFT) algorithm. The Q operation is applied, by simple multiplication, causing a change in the phase factor at $\Delta t/2$ due to the influence of the potential and perturbed Hamiltonian. This is followed by a second P operation to evaluate the wave function Ψ after the full-step propagation time Δt . This routine is then continued over subsequent Δt time steps. An initial wave function $\Psi(z,0)$ can be chosen as the sum of arbitrary even and odd wave functions.

The energy spectrum $P(\epsilon)$ is obtained from the Fourier transform of the correlation function defined as $P_l(t) = \langle \Psi(z,0) | \Psi(z,t) \rangle$ multiplied by the Hanning window function, $W_H(t) = [1 - \cos(2\pi t/T)]/T$, in order to reduce the side lobes around the eigenvalues. Thus $P(\epsilon) = \mathcal{F}[P_l(t)W_H(t)] = \sum_n |a_n|^2 L(\epsilon - \epsilon_n)$,³ where $L(\epsilon - \epsilon_n)$ is the line shape function resulting from the finite

sampling time duration T and the window function, and a_n are given by $\Psi(z,t) = \sum_n a_n \Phi_n(z) \exp(-i\varepsilon_n t)$, Φ_n being the energy eigenfunctions. The eigenfunction associated with each energy eigenvalue is found from the Fourier transform of $\Psi(z,t)$ obtained from (2):

$$\begin{aligned} \Psi(z,\varepsilon) &= \frac{1}{2\pi} \int_{-\infty}^{\infty} \Psi(z,t) \exp(i\varepsilon t) W_H(t) dt \\ &= \sum_n a_n \Phi_n(z) L(\varepsilon - \varepsilon_n). \end{aligned} \quad (5)$$

As long as the ε_n are sufficiently separated, the associated eigenfunctions $\Phi_n(z)$ are to a good approximation given by $\Phi_n(z) = \Psi(z, \varepsilon_n) / [a_n L(0)]$.

As an example, we have calculated the energy eigenvalues for a single quantum well ($\text{Al}_{0.3}\text{Ga}_{0.7}\text{As}/\text{GaAs}/\text{Al}_{0.3}\text{Ga}_{0.7}\text{As}$) with a well thickness of 100 Å, taking mass differences into account. For an electron in the conduction band, taking a band discontinuity $\Delta\varepsilon_c = 0.21324$ eV and letting the electron energy of top at the barrier equal to 0 eV, the confined computed and analytical (in parentheses) eigenvalues are -0.18357 (-0.18384) and -0.09733 (-0.09829) eV, respectively. If mass differences are neglected, these are -0.18178 (-0.18156) and -0.09322 (-0.09279) eV. The results from the BPM calculation are in excellent agreement with analytical solutions for both cases. It is observed that mass differences do not influence the results significantly. But this will be untrue when excitonic interactions are included, because exciton binding energies typically range 5–10 meV in $\text{AlGaAs}/\text{GaAs}$ quantum wells.

To extend this technique to the analysis of excitonic effects in quantum wells subjected to an external electric field E perpendicular to layers, we have used the following Kohn–Luttinger Hamiltonian^{11,12} for optical excitations, which neglects the off-diagonal terms and the in-plane center-of-mass Hamiltonian:

$$H = H_z + H_{z_h} + H_{ex}, \quad (6)$$

where

$$\begin{aligned} H_z &= -\frac{\hbar^2}{2} \frac{\partial}{\partial z_e} \left(\frac{1}{m_{e1}} \frac{\partial}{\partial z_e} \right) + V_e(z_e) + |e| E z_e, \\ H_{z_h} &= -\frac{\hbar^2}{2} \frac{\partial}{\partial z_h} \left(\frac{1}{m_{h1}} \frac{\partial}{\partial z_h} \right) - V_h(z_h) - |e| E z_h, \\ H_{ex} &= -\frac{\hbar^2}{2\mu_{||}} \left[\frac{1}{\rho} \frac{\partial}{\partial \rho} \left(\rho \frac{\partial}{\partial \rho} \right) + \frac{1}{\rho^2} \frac{\partial^2}{\partial \phi^2} \right] - \frac{e^2}{\epsilon \sqrt{\rho^2 - (z_e - z_h)^2}}. \end{aligned} \quad (7)$$

Here $\mu_{||}$ is the reduced effective mass in the plane parallel to layers, and ρ and ϕ are the relative coordinates in the plane. $|e|$, ϵ , m_{e1} , and m_{h1} are the magnitude of electron charge, the dielectric constant, and the electron and hole effective masses along the z direction, respectively. $V_e(z_e)$ and $V_h(z_h)$ are the conduction- and valence-band potential barriers due to the heterostructure. We have used a sepa-

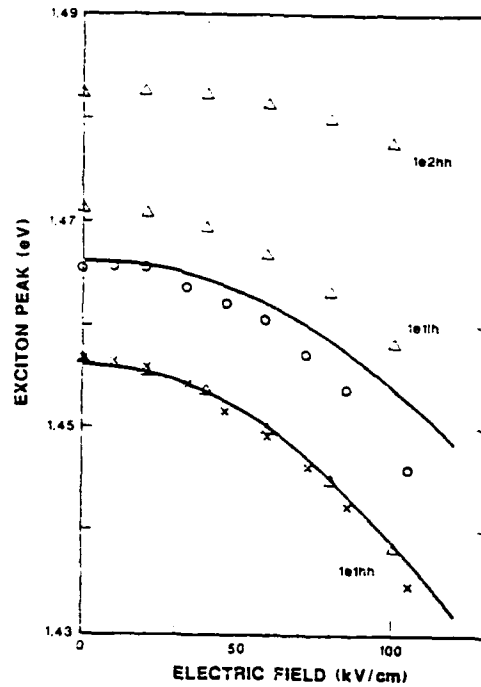


FIG. 1. Computed energies (triangles) of the 1e1hh, 1e1lh, and 1e2hh transitions obtained from the BPM and variational technique for a single quantum well ($\text{Al}_{0.32}\text{Ga}_{0.68}\text{As}/\text{GaAs}/\text{Al}_{0.32}\text{Ga}_{0.68}\text{As}$) with a well thickness of 95 Å, for various values of an electric field applied perpendicular to the layers. The crosses and circles are experimental exciton peaks taken from Ref. 4 for 1e1hh and 1e1lh transitions, respectively, and the solid lines are their calculated values.

table trial wave function to apply the variational method: $\Phi(z_e, z_h, \rho, \phi) = f(z_e)g(z_h)h(\rho, \phi)$ letting $h(\rho, \phi) = \sqrt{2/\pi} \exp(-\rho/\lambda)/\lambda$, ε_z , $f(z_e)$ and ε_z , $g(z_h)$ are obtained using the BPM as above solving $H_z f(z_e) = \varepsilon_z f(z_e)$ and $H_{z_h} g(z_h) = -\varepsilon_z g(z_h)$, respectively. Then the exciton binding energy is calculated by minimizing $\varepsilon_{ex} = \langle \Phi | H_{ex} | \Phi \rangle$.

Figure 1 shows our computed results compared to Miller *et al.*⁴ for a single quantum well ($\text{Al}_{0.32}\text{Ga}_{0.68}\text{As}/\text{GaAs}/\text{Al}_{0.32}\text{Ga}_{0.68}\text{As}$) with a well thickness of 95 Å. The initial wave function was chosen to be $\Psi(z,0) = A(1 + 2z/d) \exp(-z^2/d^2)$, where A is a normalization constant and d is half of the well thickness. We have good agreement with their experimental results. Note that the strain shift of ~ 4.5 meV for the light hole exciton peak has not been subtracted in our calculation. In addition to resonant tunneling devices, such structures are of interest as new coherent light emitters based upon superradiance from condensed exciton states in confined structures under the influence of applied fields.¹³ Thus we have also applied our BPM analysis to a double quantum well. The computed energy eigenvalues and eigenfunctions are shown in Fig. 2. Throughout the calculation, a 57.43 band discontinuity split was assumed,⁴ $\varepsilon_s = 1.424 + 1.247x$ eV, $\epsilon = 13.1 - 3x$, $m_{e1}^* = 0.0665 + 0.0835x$, $m_{eh}^* = 0.34 - 0.42x$, $m_{hh1}^* = 0.094 + 0.043x$, $m_{hh}^* = 0.115$, and $m_{hh}^* = 0.206$, where x is the Al concentration.

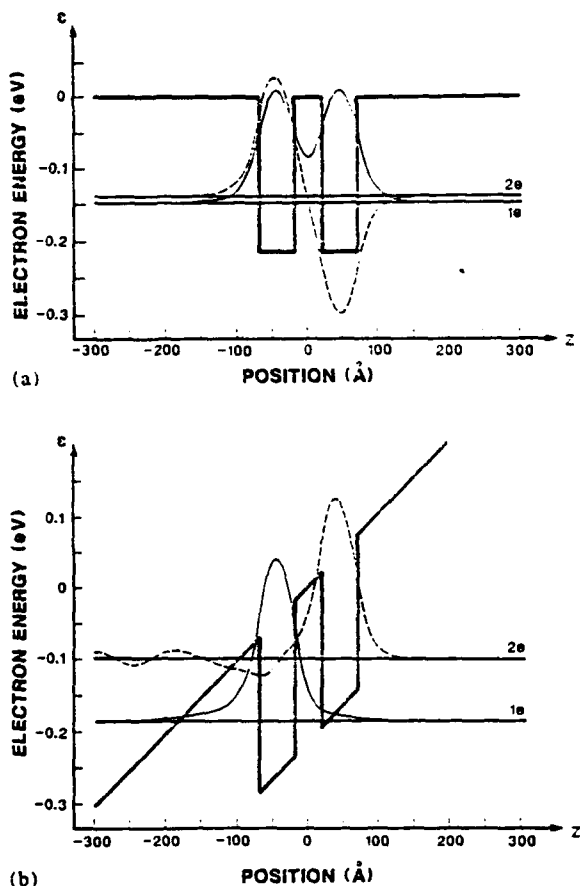


FIG. 2. (a) Energy levels and normalized wave functions from the BPM calculation are shown for an electron in the conduction band for an applied electric field of $E=0$ kV/cm, in a double quantum well ($\text{Al}_{0.3}\text{Ga}_{0.7}\text{As}/\text{GaAs}/\text{Al}_{0.3}\text{Ga}_{0.7}\text{As}/\text{GaAs}/\text{Al}_{0.3}\text{Ga}_{0.7}\text{As}$) with well thicknesses of 50/40/50 Å. 1e and 2e refer to the ground and first excited states, respectively. Energies are measured with respect to the energy level at $z=0$. An initial wave function $\Psi(z,0) = A \exp[-(z+s)^2/d^2]$ was used, where A is a normalization constant, s is the distance from $z=0$ to the center of the each well, and d is half of the well thickness. (b) Same for $E=100$ kV/cm. The ground-state wave function of (a) was used as an initial wave function.

In summary, quantum-confined structures subjected to an electric field perpendicular to layers have been analyzed using the beam propagation method and variational technique in order to investigate the quantum-confined Stark and excitonic effects. These results can be used to calculate nonlinear optical susceptibilities for various structures and to compare with experimental measurements.

One of the authors (IK) would like to acknowledge helpful discussions with J. Berkman of the Central Computing Services, University of California at Berkeley. This work was supported partially by the Air Force Office of Scientific Research (P. D., H. R. Schlossberg) Acct. No. 1-442427-22514; Ericsson Telecom AB, Sweden, Acct. No. 1-442427-54833; and the National Science Foundation (P. D., A. Harvey) Grant No. 1-442427-21520.

- ¹ M. D. Feit and J. A. Fleck, Jr., *Appl. Opt.* **17**, 3990 (1978).
- ² A. Neyer, W. Mevenkamp, L. Thylén, and B. Lagerström, *IEEE J. Lightwave Technol.* **3**, 635 (1985).
- ³ M. D. Feit, J. A. Fleck, Jr., and A. Steiger, *J. Comp. Phys.* **47**, 412 (1982).
- ⁴ D. A. B. Miller, D. S. Chemla, T. C. Damen, A. C. Gossard, W. Wiegmann, T. H. Wood, and C. A. Burrus, *Phys. Rev. B* **32**, 1043 (1985).
- ⁵ G. Bastard, E. E. Mendez, L. L. Chang, and L. Esaki, *Phys. Rev. B* **28**, 3241 (1983).
- ⁶ K. Nakamura, A. Shimizu, M. Koshihara, and K. Hayata, *IEEE J. Quantum Electron.* **25**, 889 (1989).
- ⁷ S. C. Hong, M. Jaffe, and J. Singh, *IEEE J. Quantum Electron.* **23**, 2181 (1987).
- ⁸ D. C. Hutchings, *Appl. Phys. Lett.* **55**, 1082 (1989).
- ⁹ R. L. Green and K. K. Bajaj, *J. Vac. Sci. Technol. B* **1**, 391 (1983).
- ¹⁰ D. J. BenDaniel and C. B. Duke, *Phys. Rev.* **152**, 683 (1966).
- ¹¹ J. M. Luttinger and W. Kohn, *Phys. Rev.* **97**, 869 (1955).
- ¹² J. M. Luttinger, *Phys. Rev.* **102**, 1030 (1956).
- ¹³ T. Fukuzawa, T. K. Gustafson, and E. Yamada, *IEEE J. Quantum Electron.* **26**, 811 (1990).

Self-aligned optical heterodyne experiment

(Khanh Nyguyen, Eddie Yin, Alex Spirdon (SRI), Ratnackar Neurgaonkar (Rockwell), Steven Yee (Lockheed))

(demonstrated using four-wave mixing with the photorefractive effect in Strontium barium niobate. (Presented at the Hawaii conference on NLO - July 1990). Two Master's degree reports have been written (Khanh Nyguyen and Robert Sanchez (presently at H.P.)).

Main Results

- Acceptance Angle - 40 degrees.
- Within 3 db of the ideal limit.
- Fiber spatial filtering to obtain a better match of phase fronts.

Conclusions

- Need faster crystal to allow changing coherence between pilot and signal. We are calculating numbers for quantum well material at this point. This looks promising.
- Are studying sampled photorefractive grating writing using a mode-locked argon ion laser. By timing the laser pulses periodically to a megahertz (80) signal we are attempting to demonstrate that we can store multiple high frequency patterns and readress them.

Publications

- (Wide-angle self-aligning heterodyning with four wave mixing, *Optics Letters*, 16, 1811 (1991)).
- (Self-Aligning optical Heterodyne with Four-Wave Mixing, K. Nguyen, T. K. Gustafson, T. K. Yee, and R. Neurgaonkar, presented at Nonlinear Optics, Materials,

Phenomena, and Devices, Stouffer Waiohai Beach, Kauai, Hawaii, 11-20 July 1990.)

Wide-angle self-aligning heterodyning with four-wave mixing

Khanh Nguyen, Robert Sanchez, and T. K. Gustafson

Department of Electrical Engineering and Computer Science, University of California, Berkeley, Berkeley, California 94702

T. K. Yee

Lockheed Missile and Space Company, Inc., 1111 Lockheed Way, Sunnyvale, California 94089-3504

R. Neurgaonkar

Rockwell International Science Center, Thousand Oaks, California 91360

Received June 10, 1991

Self-aligning optical heterodyning is demonstrated with an acceptance angle as large as 40° . The receiver consists of a strontium barium niobate (SBN) crystal, a detector, and collecting lenses. The incoming beam interferes with the local oscillator to create a real-time grating in the SBN crystal, which diffracts and aligns the signal with the local oscillator. Heterodyne detection occurs as long as the written grating can diffract the input signal. All alignment requirements between the signal and local oscillator are automatically satisfied by the diffraction process, which permits the large acceptance angle. Insensitivity with respect to crystal orientation and background radiation has also been demonstrated.

Heterodyne detection is a powerful method for coherent detection of weak signals. However, it places stringent requirements on the alignment of the local oscillator (LO) and the signal, in tilt, in phase front, and in position.¹⁻³ For efficient mixing, the two beams must intersect within a solid angle of $\Omega \approx \lambda^2/A$, where A is the area of the detector,⁴ and the phase fronts of the two mixing beams must be matched. These requirements reduce the effectiveness of heterodyne detection in situations in which the direction of the incoming signal is either uncertain or varying with time. Direct detection is simpler and would circumvent the alignment requirements, but it suffers from a low signal-to-noise ratio and is susceptible to background radiation.

We have demonstrated an optical heterodyne receiver with acceptance angle as large as 40° and low sensitivity to background radiation. The receiver utilizes a real-time grating written in Ce-doped strontium barium niobate (SBN) to align the signal automatically with the LO. It is also insensitive to crystal orientation. A homodyne detection experiment using a similar arrangement was performed by de Monchenault and Huignard.⁵

The experimental arrangement is shown in Fig. 1. An Ar⁺ laser operating at 514.5 nm served as the source for the experiment. The receiver is made up of the LO, the SBN crystal, and the detector together with some collecting lenses. The input beam, on entering the crystal, interferes with the LO and creates a real-time grating in the crystal via through the photorefractive effect. This grating then diffracts the signal and aligns it with the LO. Heterodyne detection occurs as long as the written grating can diffract the incoming signal. The alignment requirements between the signal and LO, in phase

front, position, and tilt, are automatically satisfied by the diffraction process. This is an advantage over conventional heterodyning, in which the two beams must cross within a solid angle of $\approx \lambda^2/A$. Wide-field-of-view direct detection, on the other hand, would be sensitive to background radiation.

The input beam is actually made up of two components, the pilot⁶ and the signal. The pilot interferes with the LO to create the real-time grating, and the signal diffracts off this grating, aligns itself with the LO, and generates the heterodyne signal. As a result, the heterodyne signal would be at $\Delta\omega = \omega_{\text{pilot}} - \omega_{\text{signal}}$. In our experiment, a frequency difference of 40 MHz between the pilot and the signal was imposed by an acousto-optic modulator.

For efficient mixing, the phase front of the diffracted signal must match that of the LO. Hence the phase front of the pilot must match that of the signal. To ensure this, both the pilot and the signal are sent into a single-mode fiber at the transmitter end before being sent to the receiver. The fiber then acts as a filter for matching the spatial modes of the pilot and the signal beams. Furthermore, owing to the relative slow response time of SBN, ω_{pilot} is made equal to ω_{LO} , which results in a stationary interference pattern that can be reproduced in the crystal. Note that a crystal with faster time response, if available, would allow the receiver to operate with $\omega_{\text{pilot}} \neq \omega_{\text{LO}}$ and would make it insensitive to frequency drift owing to the Doppler effect.

All three beams are extraordinarily polarized (Fig. 2). The signal beam is *e* polarized to maximize the diffraction efficiency by taking advantage of the largest electro-optic coefficient in SBN, r_{33} . The LO and pilot are also *e* polarized because the diffracted signal beam and the LO must have the

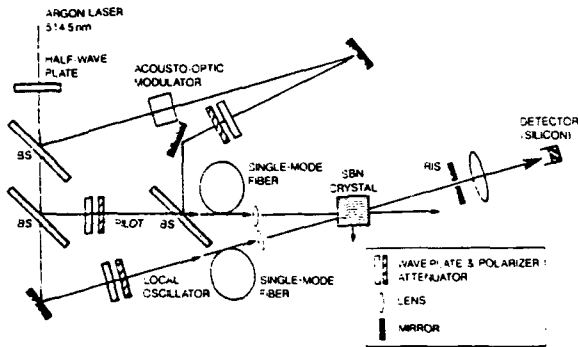


Fig. 1. Wide-acceptance-angle heterodyne detection experiment involving three laser beams at $\lambda = 514.5$ nm: signal, pilot, and LO. The signal frequency is shifted by 40 MHz by an acousto-optic modulator. Single-mode, polarization-preserving fiber is used to ensure mode matching between pilot and signal. The output, containing the LO and the diffracted signal, is focused onto the detector. BS's, beam splitters.

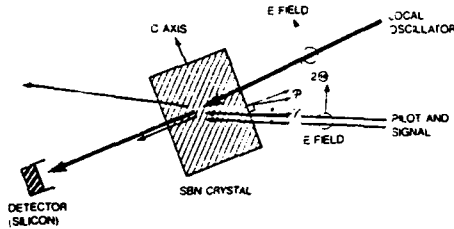


Fig. 2. Geometry of the diffraction process. Coupling is away from the C axis because electrons are the primary carriers. All three beams are e polarized to take advantage of the largest electro-optic coefficient of SBN, r_{33} . The external beam crossing angle θ and rotation angle ϕ are shown. 2θ , input angle (signal-LO angle); ϕ , rotation angle (crystal face normal-input beam angular bisector angle); γ , grating plane-signal angle.

same polarization, and cross-polarization coupling is not possible in SBN. The relative intensity of the beams is controlled by wave-plate/polarizer combinations, as shown in Fig. 1.

All beams are focused into the SBN crystal by microscope objectives. The output beam, which consisted of three collinear components, the diffracted signal, the pilot, and the LO, is collected by a lens and focused onto a detector connected to a spectrum analyzer. The only alignment necessary is to ensure that the beams intersect inside the crystal.

The grating was formed in the SBN crystal through the photorefractive process, which involves charge excitations from traps and their migration by diffusion to create a space-charge field that has the spatial distribution of the illumination.^{7,8} The space-charge field creates the grating by inducing a refractive-index modulation through the Pockels effect. For transport by diffusion and small modulation index m , the diffraction efficiency η for a transmission phase grating is given by

$$\eta = \exp\left(\frac{-\alpha z}{\cos \gamma_i}\right) \sin^2\left[\frac{\pi d(e_2^* \Delta e_{e1})}{2\epsilon_0 \lambda n \cos \gamma_i}\right], \quad (1)$$

where α is the loss coefficient for the crystal, $e_{1,2}$ are the polarizations of the input and diffracted beams,

γ_i is the incident angle with respect to the grating planes, d is the grating thickness, and Δe is the change in the dielectric tensor caused by the space-charge field ($\Delta e = 2n\epsilon_0 \delta n$). The diffraction efficiency was calculated to be approximately 30%. This did not take fanning, reflection, and absorption losses into account, however. Unfortunately, these losses are quite large,⁹ which resulted in a measured diffraction efficiency of between 5% and 10%.

The current generated by mixing between the diffracted signal and the LO is

$$i_c(t) = 2F^{1/2} \left(\frac{e\mu}{h\nu} \right) (\sqrt{P_s P_{LO}} \cos \omega t). \quad (2)$$

F , the heterodyning efficiency with a maximum value of unity, is a function of the phase-front mismatch and misalignment between the mixing beams.² F was measured to be only 3 dB below the ideal limit. The only alignment necessary was to ensure that the input and the LO beams intersect each other inside the crystal. The detector quantum efficiency μ was measured to be $\approx 43\%$. P_{LO} and P_s are the LO and diffracted signal powers, respectively, and ω is the frequency difference between the two beams (40 MHz). The heterodyne signal strength as seen on the spectrum analyzer is proportional to $i_c^2(t)$ and thus proportional to F and P_s .

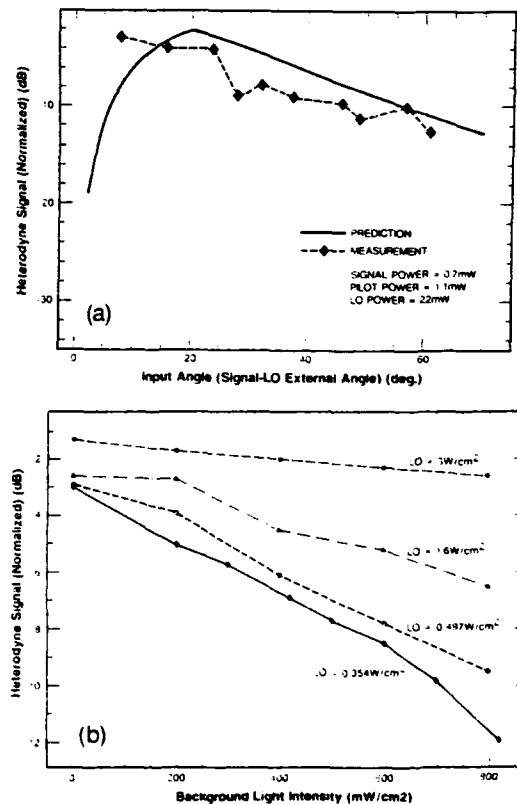


Fig. 3. Heterodyne signal dependence on signal direction, crystal orientation, and background light intensity. (a) Heterodyne signal as a function of angle θ . As the relative angle between the signal and the LO is varied from approximately 10° to 60° , the heterodyne signal shows a slight and predictable decline in amplitude of approximately 7–8 dB. (b) The effect of background light on the heterodyne signal for various LO powers.

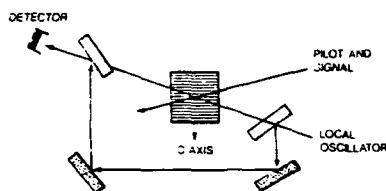


Fig. 4. Possible geometry for increasing the heterodyne signal as a function of LO.

The most desirable features of this receiver are self-alignment between the signal and LO over a wide range of acceptance angle and insensitivity to background illumination. Heterodyne detection occurs as long as the written grating can diffract the input signal. All alignments between the signal and the LO are automatically satisfied by the diffraction process. Since both the refractive-index modulation and diffraction efficiency are functions of the LO-signal crossing angle θ , the heterodyne signal is also a function of θ , as shown in Fig. 3(a). The heterodyne signal decreases as the external crossing angle increases. The signal strength varied by roughly 10 dB as 2θ is varied from 15° to 60° , corresponding to an acceptance angle of 45° . The maximum heterodyne signal for this geometry should be obtained for a crossing angle between 15° and 25° . The angle for peak diffraction efficiency and slope of the curve will be different for different crystals, depending on such factors as effective charge density N_{eff} , effective electro-optic coefficient r_{eff} , and the hole-electron competition factor $\zeta(K)$.

The receiver robustness with respect to background radiation was also demonstrated. Since the position of the LO with respect to the detector is fixed, and the signal aligns itself along the LO's direction, the detector can be shielded from most of the background light that enters the crystal. Even if the background radiation has roughly the same frequency as the signal and enters the crystal at nearly the same angle, its spatial mode is likely to be different from that of the signal. Therefore only a negligible amount would be diffracted by the grating. As a result, the effect of background radiation on the detector is negligible.

More significantly, background light affects the receiver's performance by decreasing the modulation depth of the grating and reducing its diffraction efficiency. The formation of the grating is a dynamic process in which charges are continually reexcited and trapped. The grating is formed through competition between the modulated part of the illumination and the unmodulated part. As a result, the refractive-index modulation δn is linearly dependent on m , the ratio of modulated light over the unmodulated light. Since the excitation of charges is an incoherent process, the additional background light translates to a decrease in m in accordance with the relation

$$m = \frac{2\sqrt{I_{\text{pilot}} I_{\text{LO}}}}{I_{\text{pilot}} + I_{\text{LO}} + I_{\text{background}}} \quad (3)$$

The behavior of the heterodyne signal as a function of background light for different LO powers is displayed in Fig. 3(b). For comparison, the mean intensity of solar radiation just beyond the Earth's atmosphere is approximately 140 mW/cm^2 . As predicted, the detected signal decreases with increasing background radiation. The decrease is rapid for low LO power, and gradual and small for high LO power. The robustness of the receiver with respect to background radiation is dependent on the power of the LO—the more power available to the LO, the more robust the receiver-versus-background light.

The sensitivity of the receiver depends primarily on the diffraction efficiency of the grating written in the photorefractive crystal. Therefore, the receiver sensitivity depends on the material properties of the crystal—absorption, carrier density, electro-optic constant, etc.—and m , the ratio between LO power and pilot power. For $m \approx 1$, or $P_{\text{LO}} \approx P_{\text{pilot}}$, maximum diffraction efficiency is obtained. However, large LO power is desired for shot noise to become the dominant noise in the detection process. A possible geometry to increase the heterodyne signal is shown in Fig. 4. In this geometry, the LO is split into two parts. One part of the beam is directed into the crystal to interact with the pilot and the signal. Its power would be adjusted for high diffraction efficiency. The rest of the beam could bypass the crystal and be recombined with the LO before entering the detector. With this arrangement, both high diffraction efficiency and large LO power can be achieved. Care must be taken to ensure that the phase fronts of the two LO components are well matched. Research is planned to evaluate the effectiveness of this configuration.

In conclusion, we have implemented a self-aligning optical heterodyne receiver using four-wave mixing in Ce-doped SBN. The receiver was shown experimentally to have a wide acceptance angle, exceeding 40° , and is robust with respect to background radiation and crystal orientation. Such a detection scheme has potential applications in optical communications, in situations with high background radiation and with the direction of the incoming signal either unknown or varying in time.

References

1. O. E. Delange, *IEEE Spectrum* **5**, 77 (1968).
2. O. Andrade and B. J. Rye, *J. Phys. D* **7**, 280 (1974).
3. O. Mandel and E. Wolf, *J. Opt. Soc. Am.* **65**, 415 (1975).
4. A. E. Siegman, *Appl. Opt.* **5**, 1588 (1966).
5. H. de Monchenault and J. P. Huignard, *J. Appl. Phys.* **63**, 624 (1988).
6. The name pilot was arrived at during a personal discussion with R. Bondurant of Lincoln Laboratory, Lexington, Mass.
7. R. A. Fisher, *Optical Phase Conjugation* (Academic, New York, 1983).
8. N. V. Kukhtarev, V. B. Markov, S. G. Odulov, M. S. Soskin, and V. L. Vinetskii, *Ferroelectrics* **22**, 961 (1979).
9. J. Hong, P. Yeh, D. Psaltis, and D. Brady, *Opt. Lett.* **15**, 344 (1990).

Renormalization concepts applied to strong-field NLO

(Olga Blum and Inho Kim, P. L. Kelley).

We have been investigating a new approach to treating strong-field and quantum limited nonlinear optical interactions. The basic approach was outlined in the initial proposal for quantum approaches for microstructures and involves treating pairs of field interactions rather than single interactions. This introduces the Green's functions for the radiation field modes which enter the calculation. This has its basic foundations in quantum electrodynamics but as we have shown, very useful in approaching semiclassical problems as well. Through a mutual collaboration we are completing a manuscript laying a rigorous foundations of this approach. This approach was initially applied to electro-magnetically induced transparency for NLO using an intuitive approach.

Main Results

- Treated Electromagnetically Induced Transparency
- Two strong fields and a probe field interacting with a two-level system can be obtained straight-forwardly
- Three-level system with two strong fields (draft from P. L. Kelley)

Conclusion

In collaboration with P. L. Kelley new problems are being addressed which could not be addressed with other approaches. The relationship between this approach and the dressed atom approach is being pursued. Finally we are still interested in pursuing the quantum limited case for microcavity investigations.

Publications

Application of Radiative Renormalization to Strong Field, Resonant, Nonlinear Optical Interactions, (submitted to *Phys. Rev.*) (O. Blum, T. K. Gustafson, and P. L. Kelley)

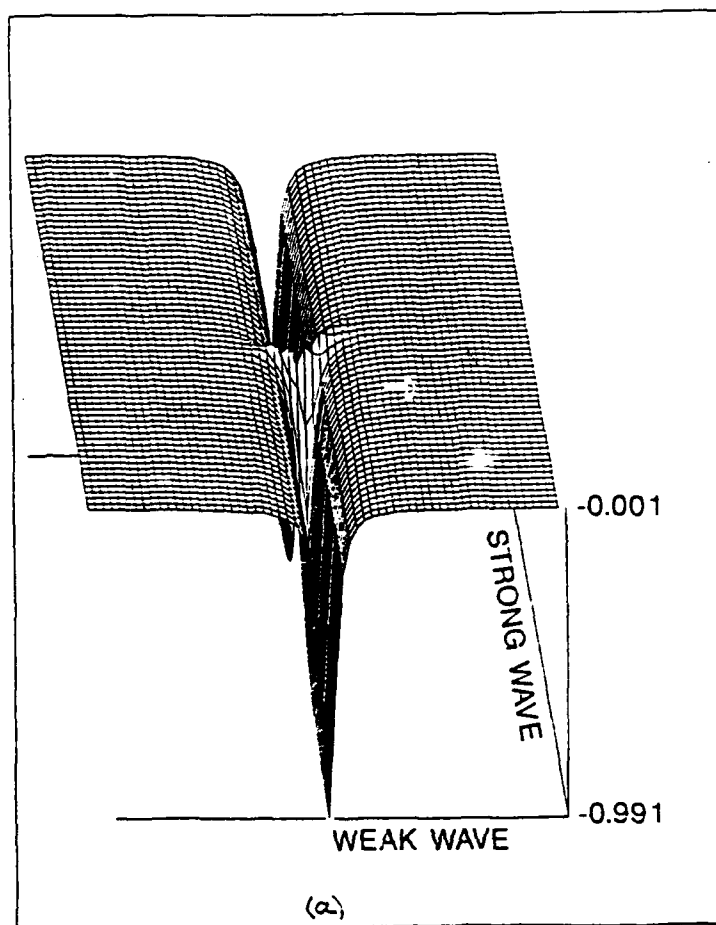
Application of Radiative Renormalization to Electromagnetically Induced Transparency, (In preparation) (O. Blum, P. L. Kelley, and T. K. Gustafson)

Radiative Renormalization in Strong Field, Resonant Nonlinear Optical Interactions, (P. L. Kelley, O. Blum, and T. K. Gustafson), (accepted for presentation at I.Q.E.C. (Vienna, June 1992))

Analysis of Third Order Parametric Processes Involving Two Strong Fields, (O. Blum, T. K. Gustafson, and P. L. Kelley), (accepted for presentation at I.Q.E.C. (Vienna, June 1992))

Weak Wave Gain versus Strong and Weak Wave Detuning

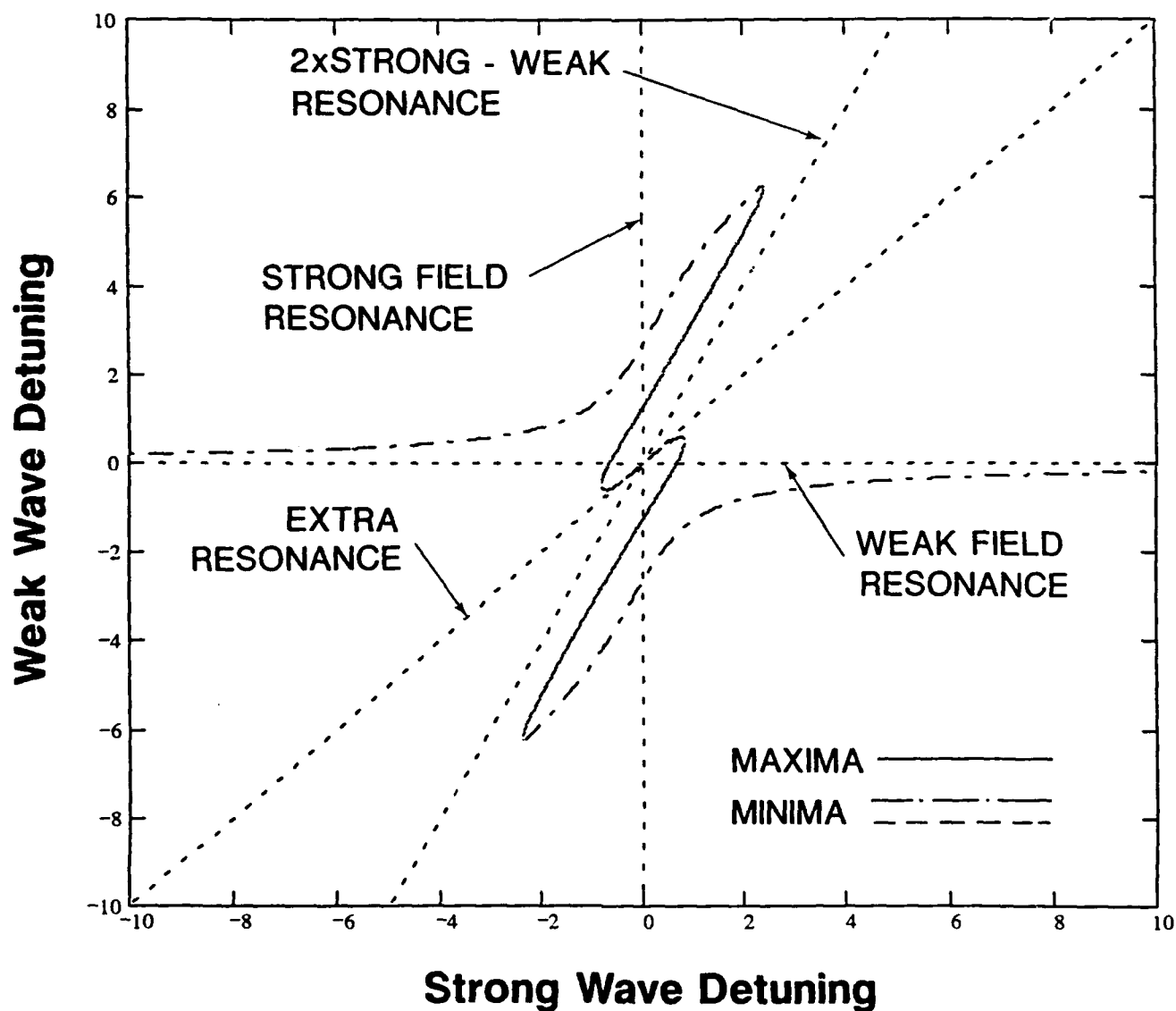
$$2\Gamma_2 = \Gamma_1 \text{ and } \Omega = .5\Gamma_1$$



Weak Stokes-field gain and loss, $\Gamma [\text{Im } \rho_{21}(nu') / \Omega']$ of a two level system excited by a strong pump beam with normalized amplitude given by $\Omega = \Gamma$. a) Surface plot of the Stokes gain and loss as a function of normalized weak field detuning $x = \nu' - \omega_0/\Gamma$ and normalized strong field detuning $y = nu - \omega_0/\Gamma$. b) Trajectories of the maxima and minima in the x - y plane. Solid lines are used for the two gain peaks, and dashed and dash-dotted lines are used for the loss peaks. Also shown are lines corresponding to the real parts of D_1 , D_2 , D_3 , and D_4 equal to zero. These are respectively $x = y$, $x = 0$, $y = 0$, and $x = 2y$.

Weak Wave Gain Maxima and Minima versus Strong and Weak Wave Detuning

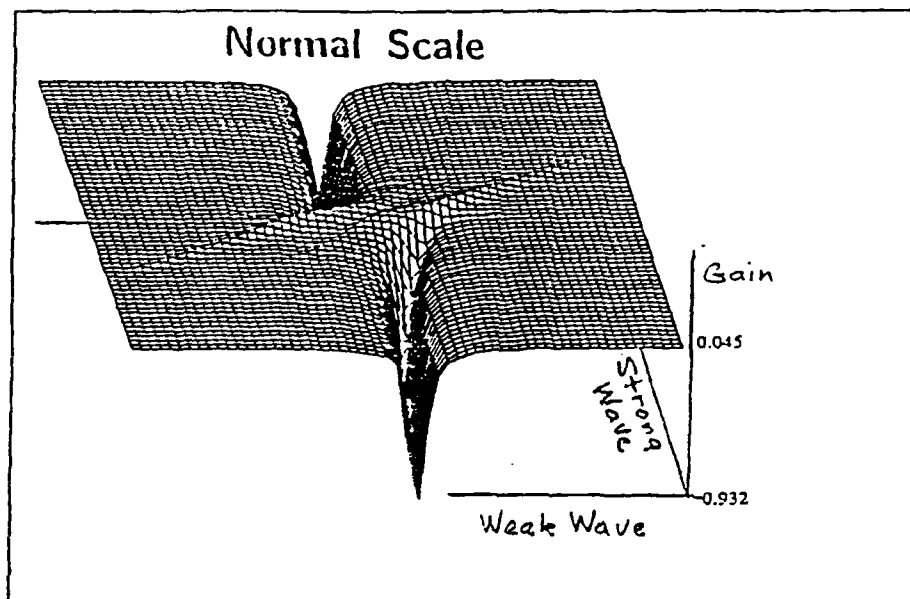
$$2\Gamma_2 = \Gamma_1 \text{ and } \Omega = .5 \Gamma_1$$



(b)

Weak Wave Gain versus Strong and Weak Wave Detuning

$$2\Gamma_2 = \Gamma_1 \text{ and } \Omega = 1.8\Gamma_1$$



Weak Stokes-field gain and loss, $\Gamma [\text{Im } \rho_{21}(nu') / \Omega']$ of a two level system excited by a strong pump beam with normalized amplitude given by $\Omega = 3.6\Gamma$. a) Surface plot of the Stokes gain and loss as a function of normalized weak field detuning $x = \nu' - \omega_0/\Gamma$ and normalized strong field detuning $y = nu - \omega_0/\Gamma$. b) Trajectories of the maxima and minima in the x - y plane. Solid lines are used for the two gain peaks, and dash-dotted lines are used for the loss peaks. Also shown are lines corresponding to the real parts of D_1, D_2, D_3 , and D_4 equal to zero. These are respectively $x = y, x = 0, y = 0$, and $x = 2y$. Curves 1, 2, 3, 4, and 5 correspond respectively to the positive minimum, the positive maximum, the extra resonance, the negative maximum, and the negative minimum, respectively.

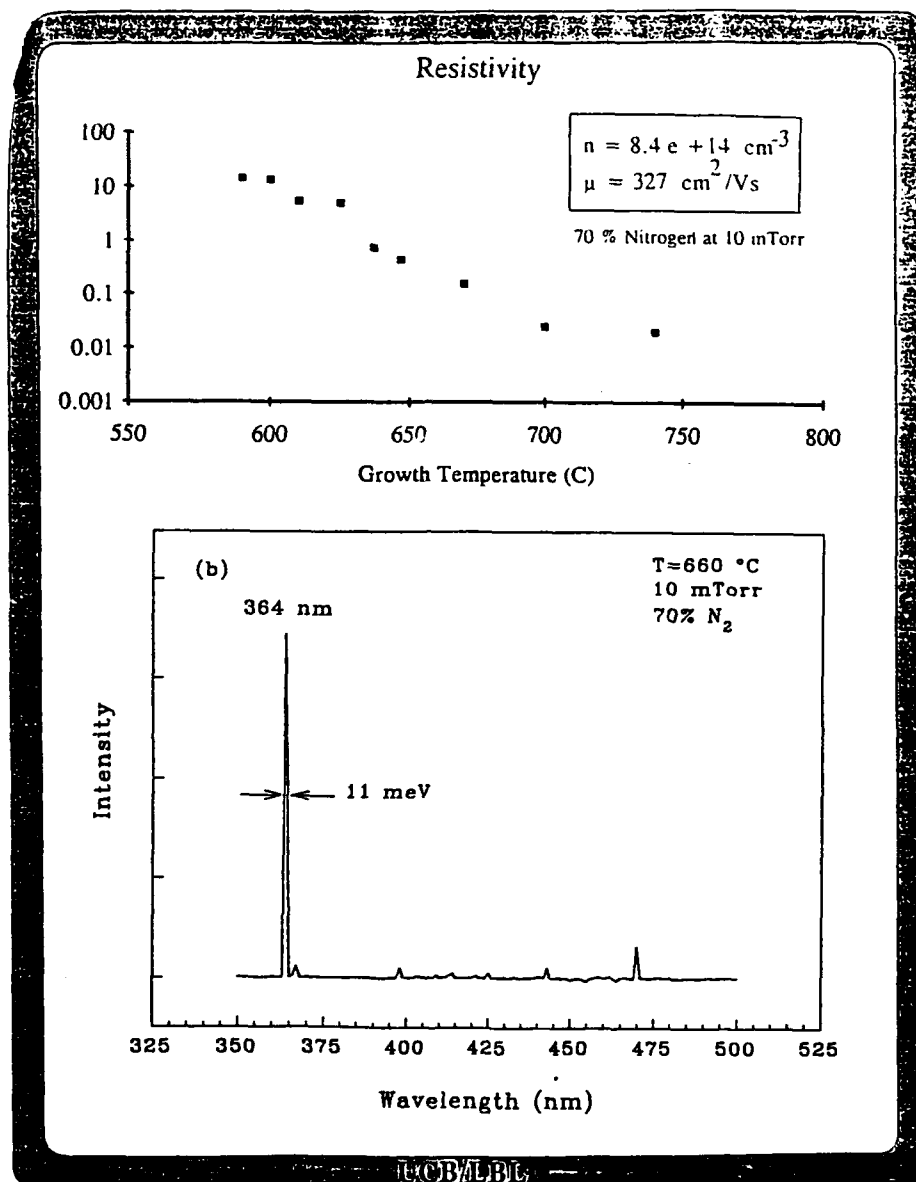
Nonlinear Optical Interactions in GaN

(Jennifer Ross, Eicke Weber, Nathan Cheung, {Mike Ruben, and Nate Neuman [the Lawrence Berkeley Laboratory]}) have been experimenting with wide band gap materials growth. In particular the latter two and Jennifer Ross: sputtering of epitaxial GaN. Several publications and conference presentations have been made discussing quality of material, stoichiometry, and the quality of material on both GaAs and sapphire substrates. Since GaN is transparent throughout the visible portion of the spectrum it is of possible interest for intersub and second harmonic generation and nonlinear optical experiments in the blue portion of the spectrum. This is an ongoing effort jointly with L.B.L. in which the nonlinear optical aspects have been of interest in relation to the grant and the materials efforts have been supported by D.O.E.

Presently a small chamber M.B.E. system is being assembled for the growth.

Conclusions

- The emphasis on this project has thus far concentrated on obtaining high quality materials. This is supported by D.O.E.
- Beam propagation method calculation of intersubband nonlinearities in progress.



Resistivity (Ωcm) and photoluminescence (room temp) of epitaxial GaN on sapphire obtained by sputtering. Hall measurements and resistivity measurements give a carrier concentration of $n = 8.4 \times 10^{14} \text{ cm}^{-3}$ and a mobility $\mu = 327 \text{ cm}^2/(\text{Vs})$. This work has been supported by DOE and a Rockwell Fellowship. With AFOSR support we have been looking at the nonlinear optical aspects.

Low Electron Photon Number Interactions

There are two aspects which we have pursued:

a) Tunable Bragg Mirrors

With the view towards fundamental studies of emission in microcavities, and in particular novel semiconductor microcavities for control over spontaneous emission properties, Olga Blum has studied the possibility of having voltage tunable distributed Bragg reflectors.

Main Results

- A voltage tunable Bragg reflector has been grown by chemical beam epitaxy that utilizes 31 periods of alternating InGaAs/InP multiple quantum well and bulk InP quarter-wave layers (joint with Jane Zucker, T. H. Chiu, M. D. Divino, K. L. Jones, and S. N. G. Chu of AT&T) has demonstrated a differential change in transmission of 14 percent at 1570 nm for an applied field of 22.5 kV/cm.

Conclusions

- To lower the necessary overall voltage and to prevent breakdown it is necessary to use interdigitated electrodes. Work has been continuing on this aspect.
- The long term goal of obtaining tunable microcavities requires two such mirrors.

b) Single Photon Detection Using the Aharonov-Bohm Effect

Recently Eddie Yin in collaboration with another student, Byoung-ho Lee and R. Y. Chaio of the physics department have investigated the possibility of using the "Time Dependent" Aharonov-Bohm Effect to:

- detect single photons

- To do quantum non-demolition measurements

Conclusions

Both of these are possible. The interaction is inherently wide band and the detection should be accomplished on the femtosecond scale with Aharonov-Bohm loops having dimensions of the order of a wave-length.

Publications

Analysis of the Aharonov-Bohm Effect Due to Time Dependent Potentials, (B. Lee, E. Yin , R. Y. Chiao, and T. K. Gustafson) (accepted for publication, *Phys. Rev.*)

InGaAs/InP multiple quantum well tunable Bragg reflector

O. Blum,^{a)} J. E. Zucker, T. H. Chiu, M. D. Divino, K. L. Jones, S. N. G. Chu,^{b)}
and T. K. Gustafson^{a)}
AT&T Bell Laboratories, Holmdel, New Jersey 07733

(Received 9 July 1991; accepted for publication 9 September 1991)

We demonstrate a voltage-tunable distributed Bragg reflector grown by chemical beam epitaxy that utilizes 31 periods of alternating InGaAs/InP multiple quantum well and bulk InP quarter-wave layers. We obtain a differential change in transmission of 14% at 1570 nm wavelength for an applied field of 2.25×10^4 V/cm. We find good agreement between the experimental results and transmission spectra calculated using the optical transmission matrix method.

Surface emitting lasers (SELs) show great potential for application in optical communications, interconnects, and information processing. Future developments toward SEL tunability, switching and beam steering require advances in surface-normal elements including modulators, Fabry-Perot (FP) structures, and distributed Bragg reflectors (DBRs). In addition, novel semiconductor microcavities¹ have attracted attention for control over spontaneous emission properties. This application also relies on availability of integratable, tunable, surface-normal geometry mirrors and filters.

In this letter, we present the first InGaAs/InP multiple quantum well (MQW) voltage-tunable Bragg mirror. Unlike the well-studied FP-type devices,²⁻⁴ in which reflectivity is changed by electro-optic effects in the spacer region between the mirrors, the DBR described here is tuned by field-induced changes in the optical properties of the quarter-wave ($\lambda/4$) layers which comprise the mirror. This type of device is advantageous for SELs, in which tunability⁵ could be enhanced by providing separate control over the reflector, gain, and phase sections, as in the case of multisection, guided-wave semiconductor lasers.⁶

We make use of the enhanced electroabsorption⁷ and electrorefraction⁸ associated with the quantum confined Stark effect in InGaAs/InP MQWs. Previously reported tunable DBRs have used electro-optic effects in bulk GaAs/AlGaAs^{9,10} or GaAs/AlGaAs MQWs¹⁰ for operation at wavelengths at least 140 nm below the band edge. The device reported here uses resonant excitonic effects to obtain a differential change in transmission $\Delta T/T$ as large as 14% and is the first surface-normal tunable DBR to operate in the 1550 nm optical communications window.

The DBR, shown schematically in Fig. 1(a), is grown at a rate of $\sim 1 \mu\text{m/h}$ by chemical beam epitaxy (CBE) at 535 °C, with triethyl indium, trimethyl gallium, and thermally cracked pure arsine and phosphine sources. Growth temperature is monitored by optical pyrometry and background pressure was $\approx 7 \times 10^{-5}$ Torr. Each period of the 31-period DBR stack is designed as a 1219 Å bulk InP layer and a 1150 Å MQW region, which is made up of eight 72 Å InGaAs QWs and seven 82 Å InP barriers. Two

typical periods are shown in the transmission electron microscopy (TEM) micrograph of Fig. 1(b). A $200 \times 200 \mu\text{m}^2$ mesa is etched using a 1:1:1 $\text{CH}_3\text{COOH}:\text{H}_2\text{O}_2:\text{HClO}$ etch through the mirror and into the substrate with a SiO_2 mask, yielding a mesa height of 8.32 μm . Evaporated Au/Cr forms a top contact. Current-voltage (I - V_{app}) characteristics show that there is minimal current flow in the voltage range of operation: for $-17 \text{ V} < V_{\text{app}} < 0 \text{ V}$, $I < 12 \mu\text{A}$. Transmission spectra at zero bias and differential transmission measurements were performed using standard lock-in techniques with a broadband source and a Ge detector.

In order to design a DBR that uses resonant excitonic effects, we have calculated the absorption spectra α and changes in the refractive index Δn for several applied fields, as shown in Fig. 2. We use the tunneling resonance method to find energy positions, linewidths, and oscillator strengths of the $n = 1$ heavy- and light-hole exciton transitions and a Kramers-Kronig transformation to obtain the corresponding quantum well refractive index n (Ref. 4) and field-induced change in refractive index Δn . In our structure, which has a total intrinsic region of 7.34 μm , the fields 0 and 2.25×10^4 V/cm correspond to $V_{\text{app}} = 0$ and 17 V, respectively.

The measured transmission of the DBR at $V_{\text{app}} = 0 \text{ V}$ is shown by the solid line in Fig. 3. Here, to facilitate comparison with the calculated mirror response (dashed line), free carrier absorption in the $1 \times 10^{18} \text{ cm}^{-3}$ n -type InP substrate, which we measure to be 20 cm^{-1} , has been subtracted. The minimum in experimental transmission occurs at 1608 nm. If there were no absorption in the structure, we would expect this stop band to be symmetric with a width of 83 nm. Due to the absorption of the MQWs, the short wavelength side of the stop band is obscured. On the long wavelength side, where absorption is minimal, interference fringes can be clearly observed between 1700–1800 nm.

To calculate the transmission of the Bragg mirror, the optical transmission matrix method¹¹ was used. We included the MQW absorption as shown in Fig. 2(a). The refractive index of the MQW was estimated using the layered-dielectric approximation¹² and the curves shown in Fig. 2(b). The optical parameters for bulk InGaAs and InP are taken from the literature.¹³⁻¹⁵ From the TEM mi-

^{a)}Department of Electrical Engineering and Computer Science, University of California, Berkeley, CA 94720.

^{b)}AT&T Bell Laboratories, Murray Hill, New Jersey 07974.

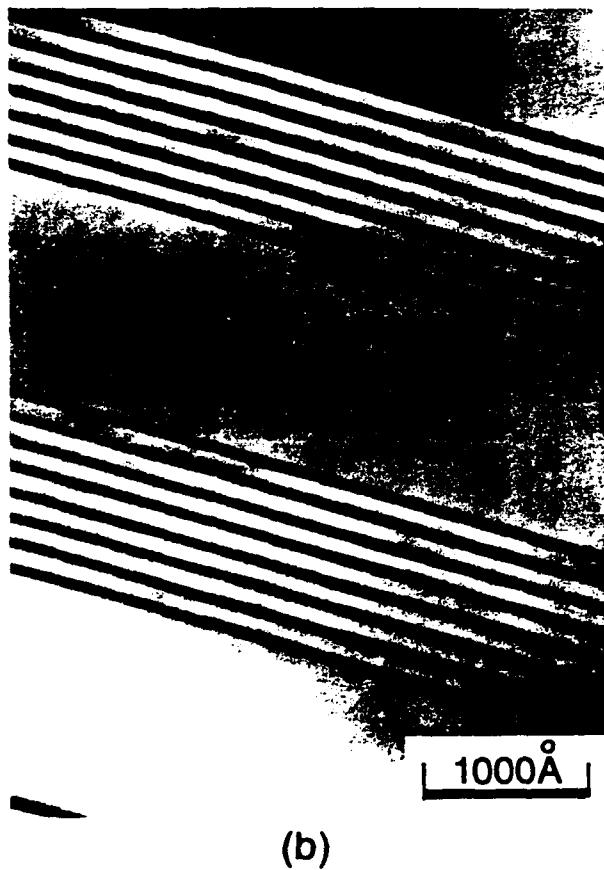
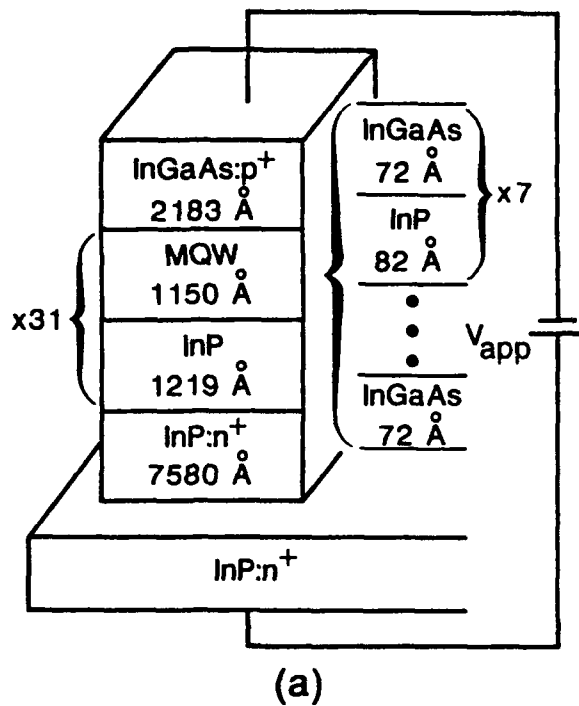


FIG. 1. (a) DBR layer structure (b) TEM micrograph of two DBR periods. The p -InGaAs cap layer has Be doping of $1 \times 10^{18} \text{ cm}^{-3}$ while the n -InP has Si doping of $1 \times 10^{18} \text{ cm}^{-3}$.

crograph taken at several points in the 31-period stack, we observed that the actual dimensions of the thick $\lambda/4$ InP layer fall in the range 1290–1350 Å. This has the effect of shifting the center of the stop band from the designed 1550

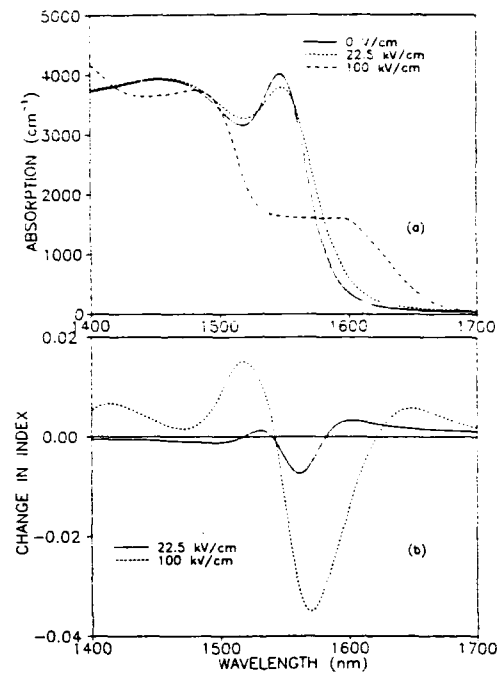


FIG. 2. (a) Calculated absorption spectrum for the 72 Å/82 Å InGaAs/InP quantum wells at applied fields 0, 2.25×10^4 , and $1.0 \times 10^5 \text{ V/cm}$. (b) Calculated refractive index change for applied fields 2.25×10^4 and $1.0 \times 10^5 \text{ V/cm}$.

to 1608 nm. In addition, the variation in thickness due to a small drift in the growth temperature from bottom to top of the DBR stack makes the stop-band asymmetric and broader. These effects are included in our calculation, shown by the dotted line in Fig. 3. We find good agreement with the measured spectrum.

When -17 V is applied to the structure, we obtain the $\Delta T/T$ spectrum shown in Fig. 4 by the solid line. The calculated $\Delta T/T$ using the α and Δn spectra of Fig. 2 is shown by the dotted line. The maximum change in experimental transmission reaches 14% at 1570 nm. The calculated spectrum shows that at this wavelength the modula-

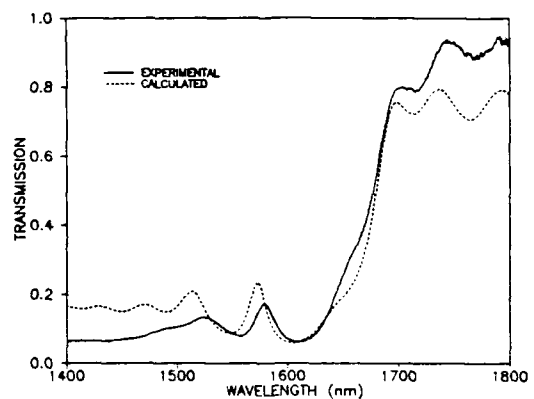


FIG. 3. DBR transmission at zero applied field. Solid line is measured, dashed line is calculated on the basis of the absorption spectrum shown in Fig. 2, the associated refractive index spectrum and the measured thickness variations.

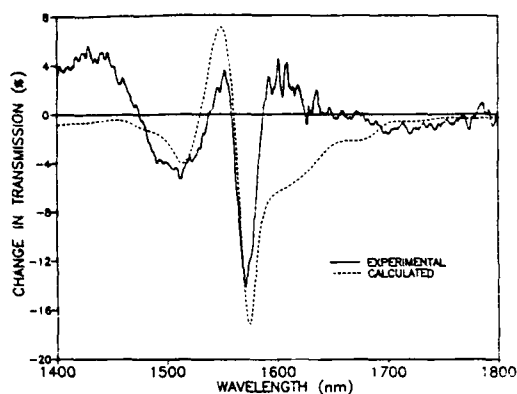


FIG. 4. Differential transmission spectrum for an applied field of 2.25×10^4 V/cm. Solid line is measured, dashed line, calculated. In the calculated spectrum α and n from Fig. 2 are used.

tion is mostly due to the electroabsorption associated with the red shift of the $n = 1$ heavy hole exciton. The feature at 1474 nm is likewise associated with the shift and broadening of the $n = 1$ light hole exciton. In the calculated spectrum we neglect the nonresonant Franz-Keldysh effects from the bulk InP,¹⁶ since at this wavelength the magnitudes of Δn and α are much smaller than those of the MQWs. Near the $n = 1$ heavy hole resonance, there is good agreement between measured and calculated spectra. There is less satisfactory agreement between measured and calculated $\Delta T/T$ spectra in the longer wavelength region. Here defects and background impurities may cause a bandtail in the absorption spectrum that is not included in the calculated spectrum of Fig. 2.

Our analysis shows that the maximum attainable $\Delta T/T$ is closely tied to the amount of field-induced shift for the heavy-hole exciton, which in turn depends on maximum voltage that can be applied. Experimentally, we were limited to 17 V by reverse-bias breakdown in our $p-i-n$ diode. Thus our maximum applied field was only 2.25×10^4 V/cm, producing a small shift as shown in Fig. 2(a) (dotted line). If a larger field could be applied, e.g., 10^5 V/cm, a much larger shift could be achieved. This is shown by the estimated absorption spectrum, indicated by the dashed line in Fig. 2(a). In order to obtain an applied field of this magnitude using the present contacting scheme, a voltage of 73.4 V would be required. Clearly such a large voltage is not practical. However, by employing a selective contact scheme^{9,17} to each $\lambda/4$ layer, application of only ~ 1 V would result in the desired field of 10^5

V/cm. Using the same method as that for the calculated $\Delta T/T$ spectrum shown in Fig. 4, but with values of α and n corresponding to a field of 1×10^5 V/cm, we would expect a significant improvement, $\Delta T/T \approx 100\%$ at 1556 nm.

In summary, we have demonstrated the first tunable surface-normal DBR for optical communications wavelengths. We use electroabsorption and electrorefraction in InGaAs/InP quantum wells to obtain $\Delta T/T = 14\%$ for 2.25×10^4 V/cm, a field one order of magnitude smaller than that in previously demonstrated structures. We successfully model the transmission and differential transmission using the optical matrix method, with quantum well absorption and refraction taken into account.

We wish to acknowledge helpful discussions with G. Livescu, O.B. and T.K.G. were supported by the Newport Fellowship, National Science Foundation, and the Air Force Office of Research. Some fabrication was performed at the University of California at Berkeley Microelectronics Laboratory.

¹Y. Yamamoto, S. Machida, and O. Nilsson, *Phys. Rev. A* **34**, 4025 (1986).

²M. Whitehead, A. Rivers, G. Parry, J. S. Roberts, and C. Button, *Electron. Lett.* **25**, 984 (1989).

³R. H. Yan, R. J. Simes, and L. A. Coldren, *IEEE Photon. Technol. Lett.* **2**, 118 (1990).

⁴G. Livescu, G. D. Boyd, L. M. F. Chirovsky, A. M. Fox, R. A. Morgan, R. E. Leibenguth, M. T. Asom, and M. W. Focht, in *Conference on Lasers and Electro-optics* (Optical Society of America, Washington, DC, 1991), pp. 44-46; G. D. Boyd and G. Livescu, *Opt. Quantum Electron.* (to be published); G. D. Boyd, G. Livescu, L. M. F. Chirovsky, and A. Mark Fox, in *OSA Proceedings on Photonic Switching*, edited by H. Scott Hinton and Joseph W. Goodman, March 6-8, 1991, Salt Lake City, Utah, Vol. 8, 222-226.

⁵C. Chang-Hasnain, J. P. Harbison, C. E. Zah, L. T. Florez, and N. C. Andreadakis, *Electron. Lett.* **27**, 1002 (1991).

⁶T. L. Koch and U. Koren, *J. Lightwave Technol.* **8**, 274 (1990).

⁷I. Bar-Joseph, C. Klingshirn, D. A. B. Miller, D. S. Chemla, U. Koren, and B. I. Miller, *Appl. Phys. Lett.* **50**, 1010 (1987).

⁸J. E. Zucker, I. Bar-Joseph, G. Sucha, U. Koren, B. I. Miller, and D. S. Chemla, *Electron. Lett.* **24**, 458 (1988).

⁹K. W. Goossen, J. E. Cunningham, and W. Y. Jan, *Appl. Phys. Lett.* **57**, 744 (1990).

¹⁰G. W. Yoffe, D. G. Schlom, and J. S. Harris, Jr., *Appl. Phys. Lett.* **51**, 1876 (1987).

¹¹P. Yeh, *Optical Waves in Layered Media* (Wiley, New York, 1988).

¹²J. E. Zucker, K. L. Jones, M. G. Young, B. I. Miller, and U. Koren, *Appl. Phys. Lett.* **55**, 2280 (1989).

¹³R. H. Kingston, *Appl. Phys. Lett.* **34**, 744 (1979).

¹⁴G. D. Pettit and W. J. Turner, *J. Appl. Phys.* **36**, 2081 (1965).

¹⁵H. Burkhard, H. W. Dinges, and E. Kuphal, *J. Appl. Phys.* **53**, 655 (1982).

¹⁶T. E. Van Eck, L. M. Walpita, W. S. C. Chang, and H. H. Wieder, *Appl. Phys. Lett.* **48**, 451 (1986).

¹⁷G. H. Dohler, G. Hasnain, and J. N. Miller, *Appl. Phys. Lett.* **49**, 704 (1986).

Analysis of Aharonov-Bohm Effect Due to Time Dependent Vector Potentials

B. Lee, E. Yin, T.K. Gustafson

Department of Electrical Engineering
University of California
Berkeley, CA 94720

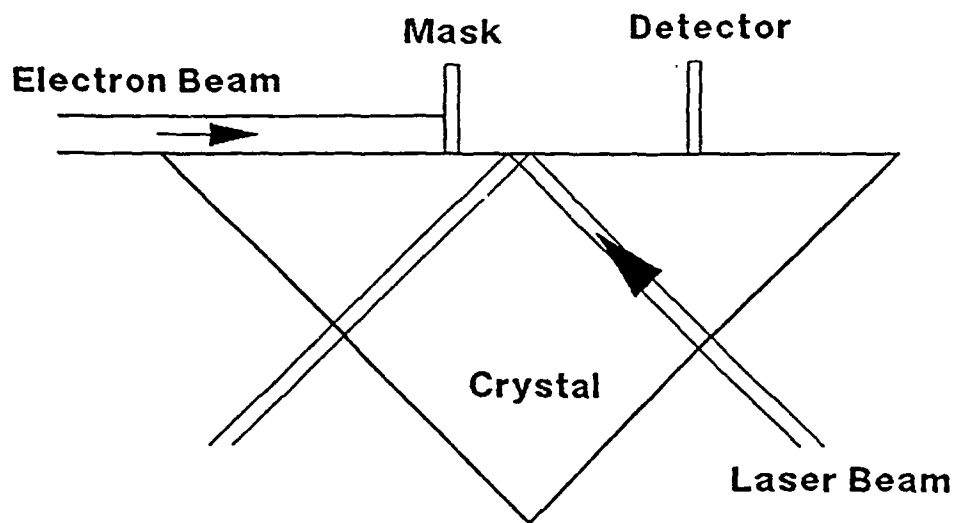
R. Chiao

Department of Physics
University of California
Berkeley, CA 94720

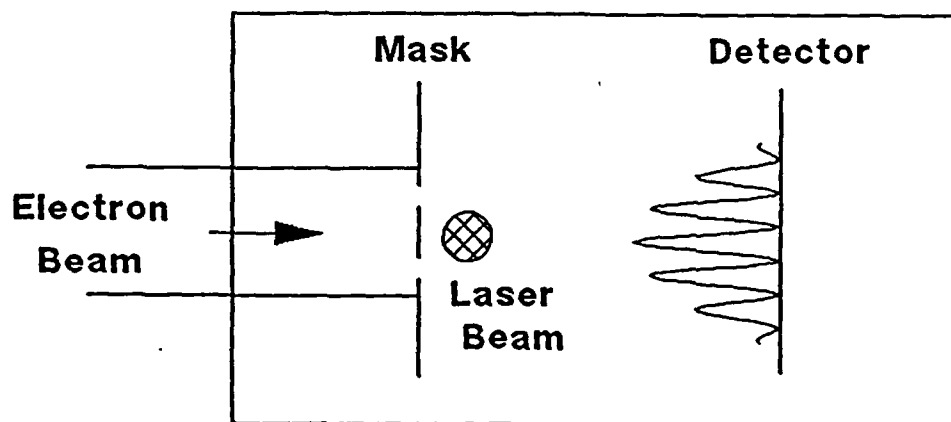
ABSTRACT

We analyze and propose a method to detect the Aharonov-Bohm effect due to time-varying vector potentials, specifically those arising from a coherent light source. We show that the effect is feasible for use as a light intensity detector. The quantum limit of detection is that of a single photon. Such a system would be a quantum non-demolition measurement since no photon absorption occurs.

November 1, 1991



Side View



Top View

Figure 4

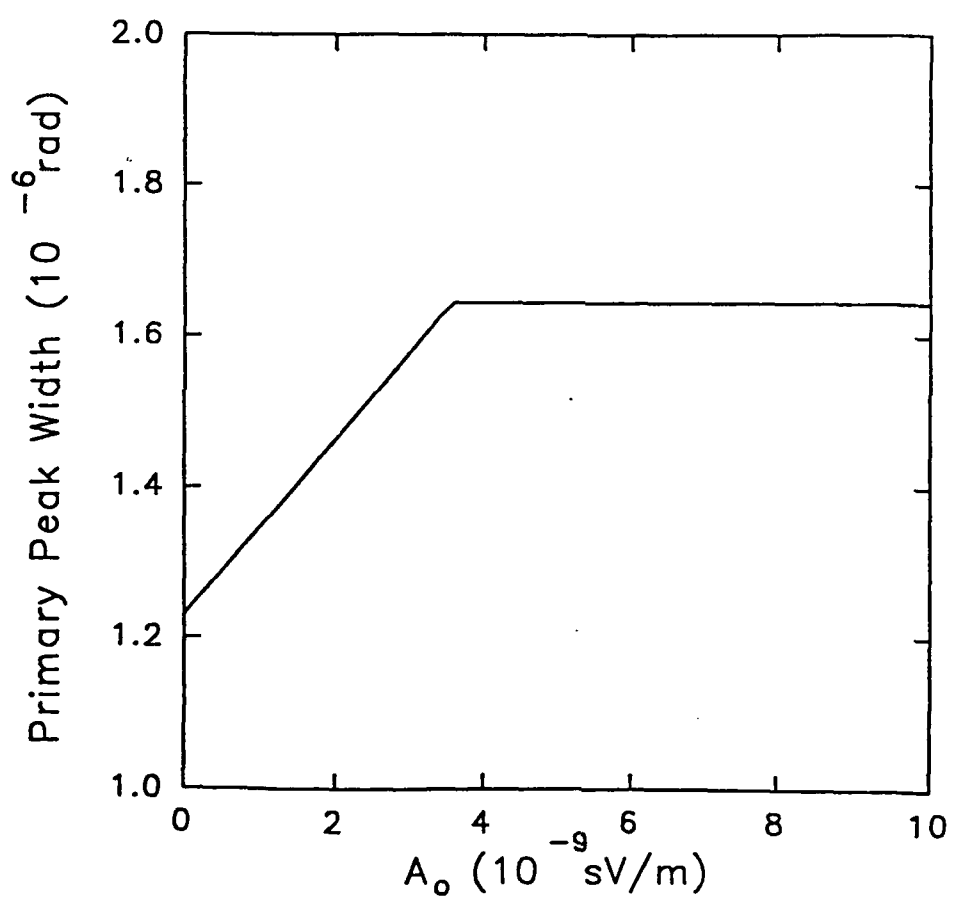


Figure 5